Research Article

INTERNATIONAL JOURNAL OF ADVANCED ROBOTIC SYSTEMS

International Journal of Advanced Robotic Systems
March-April 2020: 1–13

DOI: 10.1177/1729881420917016
journals.sagepub.com/home/arx

SAGE

Multichannel optimization for electromyogram signals with complex features in a decomposition-based multi-objective evolution framework with adaptive angle selection

Zheng Wang[1], Guoqi Chen[1], Weikun Li[1], Honghai Liu[2] and Wanliang Wang[1]

Abstract

Intelligent manufacturing is a focus of current manufacturing research, and, in combination with the Internet, it enables accurate real-time control of intelligent equipment. Highly accurate real-time prosthesis control has very important applications in therapeutics, intelligent prosthesis, and other fields. However, the applicability of the current electromyogram signal recognition method is not strong because of multiple factors. These include considering one objective (correctness) only and the inability to consider differences of recognition accuracy between actions, to recognize the number of channels, or to recognize computational complexity. In this article, we propose a multi-objective evolutionary algorithm based on a decomposition-based multi-objective differential evolution framework to construct a multi-objective model for electromyogram signals with multiple features and channels. Such channels and features are balanced and selected by using a support vector machine as an electromyogram signal classifier. Results of substantial experiment analyses indicate that the multi-objective electromyogram signal recognition method is superior to the single-objective ant colony algorithm and that the decomposition-based multiobjective evolutionary algorithms with Angle-based updating and global margin ranking is better than the decomposition-based multi-objective evolutionary algorithm and decomposition-based multiobjective evolutionary algorithms with angle-based updating strategy in handling multi-objective models for electromyogram signals.

Keywords

Multichannel optimization, multi-objective evolution, surface electromyogram signal, support vector machine classifier, adaptive angle selection

Date received: 04 September 2019; accepted: 23 February 2020

Topic: Intelligent Robot-Assisted Manufacturing
Topic Editor: Henry Leung
Associate Editor: Bin He

Introduction

Major revolutions, such as big data, cloud computing, three-dimensional printing, and industrial robots, have occurred in information technology and industrial sectors in recent years. Among these, intelligent manufacturing, as a product of in-depth fusion between information development and industrialization, has attracted wide attention from

[1] College of Computer Science and technology, Zhejiang University of Technology, Hangzhou, Zhejiang, China
[2] Intelligent Systems and Biomedical Robotics Group, School of Computing, University of Portsmouth, Portsmouth PO1 3HE, UK

Corresponding author:
Guoqi Chen, College of Computer Science and technology, Zhejiang University of Technology, Hangzhou, Zhejiang 310014, China.
Email: cgq45120@gmail.com

governments worldwide. In general, intelligent manufacturing can be regarded as a collection of manufacturing activities that integrate manufacturing and digital techniques, intelligent control technique, and networking throughout the full life cycle of design, production, management, and services.[1,2] It involves sensing, analyzing, reasoning, decision-making, and control during the manufacture process to enable a dynamic response to product demand, quick development of new products, and real-time optimization of production and the supply chain network.

Since the beginning of the 21st century, there has been explosive growth in new-generation information technology. The primary drivers of this new industrial revolution are the wide application of digital techniques, networking, and intelligent technique in manufacturing along with the constant innovations in integrated manufacturing. Intelligent manufacturing represents a development goal in 21st-century manufacturing and is a focus of current research in the field. Prostheses will be important equipment for future intelligent manufacturing.[3–6]

Human electrophysiological signals are direct responses to human behavioral intention. Analysis and interpretation of human electrophysiological signals enable a machine to recognize effectively the subjective awareness of a person.[7] As one type of human electrophysiological signal, the surface electromyogram (sEMG) signal contains information about muscle state and human motion intent. Applying gesture action recognition techniques to intelligent prostheses not only assists patients who have lost limbs in rehabilitation but also gives them a "phantom limb feel." Therefore, sEMG-based hand action recognition techniques have important medical application value.[8]

In this regard, Lu and Liu[9] performed discriminant analysis of EMG signals by integrating a nonlinear support vector machine and linear discriminant analysis, resulting in an accuracy up to 91.2%. Cai et al.[10,11] employed a wavelet transform approach to analyze features of sEMG signals of four actions, yielding a recognition accuracy of >90%. Nazarpour[12] obtained hand action features for high-order statistical calculation while running a clustering analysis of classified hand action postures, resulting in a recognition accuracy of up to 91%. Current studies focus on the classification of a single objective (recognition accuracy); that is, this technique is considered as a single-objective problem. In actual EMG signal application modeling, multiple factors such as recognition correctness, stability, and continuity should be taken into account together.

Multi-objective evolutionary algorithms (MOEAs) are metaheuristic intelligent optimization approaches simulating the natural evolution process.[13] As one set of Pareto approximate solutions can be obtained in one run alone, this type of algorithm is highly successful in multi-objective optimization field.[14] Depending on the subject survival mechanism, evolutionary multi-objective optimization algorithms can be divided into algorithms based on the Pareto governing relationship, performance indicators, and decomposition (MOEA/Ds).[15–19] MOEA/Ds convert a multi-objective optimization problem into a number of single-objective optimization subproblems. They then take advantage of information of a certain number of neighboring problems to optimize such subproblems by using an evolution algorithm. MOEA/Ds combine the conventional multi-objective mathematical programming approach and an evolutionary algorithm. By decomposing a multi-objective optimization problem into a number of single-objective optimization subproblems with a set of evenly distributed weight vectors, the evolution algorithm is then used to solve various subproblems simultaneously, thereby obtaining an evenly distributed Pareto optimal solution set. Compared with other types of algorithms, MOEA/Ds have a lower computational complexity and yield a Pareto optimal solution set with better convergence and diversity. They have thus attracted increasing attention among researchers.[20–23] Under the MOEA/D framework, an algorithm for solving the multi-objective EMG signal recognition problem was designed in this study.

First, an application-oriented multi-objective EMG signal recognition model was developed. Then the MOEA/D multi-objective solving framework was introduced into this model to solve a multi-objective problem. The structure of this article is as follows: The second section introduces the MOEA/D solution framework. The third section presents the multi-objective programming model of EMG signal recognition, the solution framework, and the application in EMG signal recognition of decomposition-based multiobjective evolutionary algorithms with angle-based updating and globalMargin ranking (MOEA/D-AU-GMR). The fourth section describes the relevant experiment.

Decomposition-based multi-objective optimization approach

In this study, an MOEA/D was utilized to optimize the subproblems. As one solution on the Pareto front corresponds to an optimal solution to each single-objective optimization subproblem, one set of Pareto optimal solutions can be eventually calculated. This approach is far superior in maintaining a solution distribution, while optimization through analyzing the information of neighboring problems can help to avoid local optima.

To convert a multi-objective problem into a set of scalar optimization problems, common decomposition methods include the weighted sum approach, the Tchebycheff[24] approach, and the boundary intersection approach. In this study, the Tchebycheff approach was used to solve four-dimensional objective problems based on a model detailed as follows

$$\begin{aligned} \min \quad & \sigma(x|\lambda, z^*) = \max\left\{\lambda_i\left(y_i(x) - z_i^*\right)\right\} \\ s.t \quad & x = \left[f_1, f_2, ..., f_{n_f}, p_1, p_2, ..., p_{n_p}\right] \\ & x \in \xi \end{aligned} \tag{1}$$

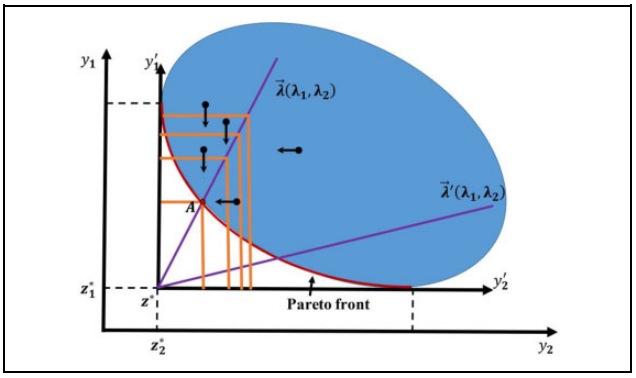

Figure 1. Pareto front of the two-dimensional minimal optimization problem.

where $z_i^* = \min(y_i(x)|x \in \xi)$ for each component, λ_i is the weight of the ith objective, and x is the $0-1$ vector consisting of the EMG signal feature and the electromyograph channel.

As shown in Figure 1, we let coordinate system y_i transform into y_i'. If any new subject y_i' appearing above $\bar{\lambda}$ is below a contour line, then both contour lines move downward simultaneously. Likewise, if any new subject y_i' appearing below $\bar{\lambda}$ is below a contour line, then both contour lines move leftward simultaneously until the Pareto front is searched.

In this study, x is subjected to differential evolution: Unlike in the genetic algorithm, mutation vectors in the differential evolution algorithm are generated by parent differential vectors and cross over with parent subject vectors to generate new subject vectors, which are directly involved in selection with their parent subjects. Obviously, the differential evolution algorithm has a more significant approximation effect than the genetic algorithm.

1. Mutation

In the ith iteration, three subjects that are different from each other, $x_{p1}(g)$, $x_{p2}(g)$, and $x_{p3}(g)$, are randomly selected from the population, where $p1 \neq p2 \neq p3$. The generated mutation vectors are then

$$H_i(g) = x_{p1}(g) + F\big(x_{p2}(g) - x_{p3}(g)\big) \quad F \in [0,1] \quad (2)$$

where $F \in [0, 1]$.

2. Crossover

Let cr be the crossover probability. The jth element X_i of the ith population $X_{ij}(g)$ is replaced by a mutation vector element when the random generation probability is less than the crossover probability in the gth iteration. Otherwise, it is an element of the original population. This situation can be expressed as

$$x_{ij}^*(g) = \begin{cases} H_{ij}(g), & \text{rand}(0,1) < \text{cr} \\ x_{ij}(g), & \text{else} \end{cases} \quad (3)$$

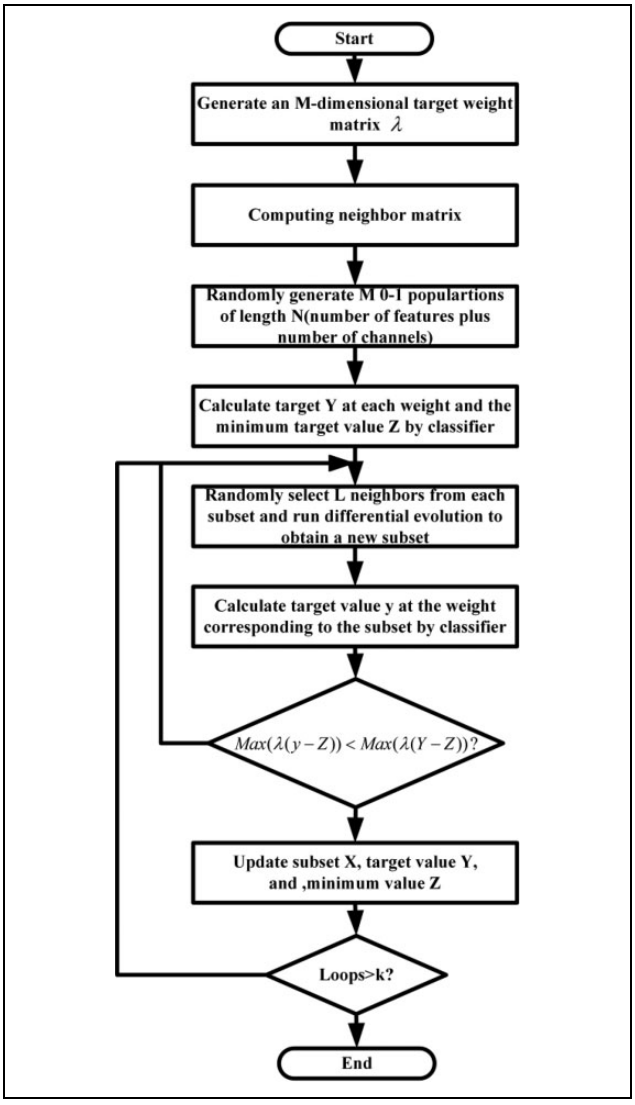

Figure 2. Basic flowchart of the MOEA/D. MOEA/D: decomposition-based multi-objective evolutionary algorithm.

We use an improved MOEA/D with adaptive angle selection (MOEA/D-AAU-GMR) to solve the problem. The basic flowchart of the MOAE/D is shown in Figure 2.

Multi-objective optimization modeling of the EMG signal classifier

Multi-objective modeling of EMG signal recognition

Selection of different channels and features will result in differences in recognition accuracy, but too many channels and features may lead to resource waste while too few channels and features will make recognition accuracy decrease too quickly. Therefore, provided that a certain threshold is guaranteed, we have the following formulas

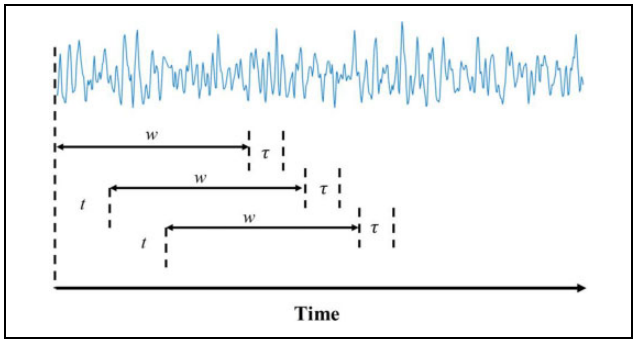

Figure 3. Window analysis method.

$$\begin{cases} p_i = \begin{cases} 1, \text{ using the } i\text{th channel} \\ 0, \text{ not using the } i\text{th channel} \end{cases} \\ f_j = \begin{cases} 1, \text{ using the } i\text{th feature} \\ 0, \text{ not using the } i\text{th feature} \end{cases} \\ n_p^u = \sum_{i=1}^{n_p} p_i \\ n_f^u = \sum_{j=1}^{n_f} f_j \\ n_{p,l}^u \le n_p^u \le n_p \\ n_{f,l}^u \le n_f^u \le n_f \end{cases} \tag{4}$$

where n_p is the total number of channels, n_f is the total number of features, $n_{p,l}^u$ is the number of the least frequently used channels, $n_{f,l}^u$ is the number of the least frequently used features, n_p^u is the number of used channels, and n_f^u is the number of used features. Consequently, constraints on the numbers of channels and features can be guaranteed at a given accuracy.

The source data of the sEMG signals acquired by the electrodes were processed by window analysis.[25] This method uses two parameters—window length and increment interval, which are associated with recognition accuracy and response time of the intelligent prosthetic system, respectively. Figure 3 illustrates the process of window analysis for one channel signal alone. w represents the window length, t represents the increment interval, and τ represents the time delay of feature extraction and classification. In this method, in every time interval t, signals within time length w as a whole are sequentially subjected to feature extraction and classification. Although the windows overlap, they are independent in terms of feature extraction and classification.

Therefore, the following definitions are introduced

$$\begin{cases} \alpha = \left[g_1, g_2, \ldots, g_{n_f} \right] \\ C^k = \alpha * D^k \end{cases} \tag{5}$$

Where α is an n_f-dimensional operator containing n_f feature calculation formulas, D^k is the EMG information value obtained from n_p channels when the kth action is being done, and $\alpha * D^k$ represents the formula for feature calculation. In other words, different feature values are calculated from information of various channels to form a feature matrix with a dimensionality of $n_f * n_p$.

The following formulas were used to select and recognize the best channel and the best feature

$$\begin{cases} P = \left[p_1, p_2, \ldots, p_{n_p} \right] \\ F = \left[f_1, f_2, \ldots, f_{n_f} \right] \\ S = F \cdot P \end{cases} \tag{6}$$

where P is defined as a channel vector consisting of p_i to represent channel usage, F is defined as a feature vector consisting of f_j to represent feature usage, and then S is the $0-1$ matrix resulting from the dot product of vectors P and F, representing use or nonuse of the channel or feature. The feature was further processed with a classifier δ to obtain a true positive result J^k, and the recognition accuracy of the kth action was calculated

$$\begin{cases} J^k = \delta\left(S \circ C^k\right) \\ P_l^{a^k}\left(J_l^k, R_l^k\right) = \begin{cases} 1, \ J_l^k = R_l^k \\ 0, \ J_l^k \ne R_l^k \end{cases} \\ a^k = \dfrac{1}{N} \sum_{l=1}^{N} P_l^{a^k} \\ a^k \ge \beta \end{cases} \tag{7}$$

where R_l^k represents correct classification of the lth sample in the kth action. $P_l^{a^k} = 1$ when $J_l^k = R_l^k$ and the judgment result is correct; otherwise $P_l^{a^k} = 0$. Summing the results of N samples gives accuracy a^k of the kth action in which β is a threshold.

To minimize the numbers of channels and features, the following objectives were established

$$\begin{cases} \min \quad n_p^u \\ \min \quad n_f^u \end{cases} \tag{8}$$

While minimizing the numbers of channels and features, a high recognition efficiency should be guaranteed and an excessively great difference in recognition accuracy between actions should be prevented

$$\begin{cases} \min \quad 1 - \dfrac{1}{n_a} \sum_{k=1}^{n_a} a^k \\ \min \quad \sqrt{\dfrac{1}{n_a} \sum_{k=1}^{n_a} \left(a^k - \dfrac{1}{n_a} \sum_{k=1}^{n_a} a^k \right)^2} \end{cases} \tag{9}$$

where n_a represents the total number of actions. While ensuring that recognition accuracy of each action is as high

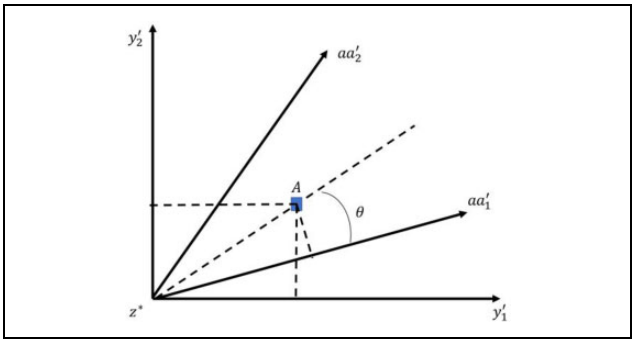

Figure 4. Illustration of the acute angle between solutions and the corresponding weight vector.

as possible, the recognition difference between actions was controlled with the standard deviation.

MOEA/D-AAU-GMR

Based on the framework of the decomposition-based multi-objective optimization algorithm, which decomposes a multi-objective optimization problem into N optimization subproblems, we propose an adaptive-angle-selection-based multi-objective optimization algorithm called decomposition-based multiobjective evolutionary algorithms with angle-based updating strategy (MOEA/D-AU), which is designed based on our previous work.[26] The algorithm adaptively adjusts the angle range selection coefficient G by using an appropriate dynamic adjustment strategy and introduces an external file set to update optimal solutions so that the algorithm focuses on convergence and then dispersion in the convergence process.

We employ the modified Tchebycheff function.[24] The function for the ith subproblem can be defined as follows

$$F(x) = \sum_{i=1}^{m} \left\{ \frac{1}{\lambda_i} \left| y_i(x) - z_i^* \right| \right\} \tag{10}$$

If $\lambda_i = 0$, λ_i is set to 10^{-6}.

Compared with MOEA/D, this algorithm changes how to choose which solution is better. In Figure 4, solution A is the current solution and aa is the corresponding direction vector, θ is the acute angle between solution A and its corresponding direction vector aa, when the weighted Tchebycheff approach is used, which also is the acute angle between vector aa and vector $F(x) - Z$.

$\theta(x)$ is denoted as $\langle aa, F(x) - Z \rangle$, which can be obtained by

$$\theta(x) = \arccos\left(\frac{aa^*(F(x) - z^*)}{||aa||^*||F(x) - z^*||} \right) \tag{11}$$

with

$$aa = 1/\lambda \tag{12}$$

The smaller the value of $\theta(x)$ is, the closer the solution x is to the direction vector aa. In this way, the solution that is close to the direction vector can be selected.

The parameter G is the number of selected angles, which varies with evolution. The dynamic adjustment strategy adopted is to gradually increase the angle control parameter G in MOEA/D-AAU-GMR with evolution as follows

$$\text{Sigmoid} : G_r = \left[\frac{G_{\max}}{1 + \exp\left[-20 \times \left(\frac{s}{S} - g \right) \right]} \right] \tag{13}$$

where $G_{\max}$ is the maximum of G_r, which is the value of G at present; s is the number of iterations at present; S is the maximum number of iterations; and $g \in [0, 1)$ is a control variable parameter used to control the growth rate of G_r.

However, while screening the solutions in this way, the algorithm may ignore some specific optimal solutions. Therefore, a global margin ranking strategy[27] was introduced to build an external file set and rank the updated solutions and original solutions based on individual margin information, resulting in individual dominance values (rank values) in the solution space, thereby retaining partial solutions. The specific formula is shown below

$$\text{GMR}(x_i) = \sum_{x_i \neq x_j} \max\left(\prod_{m=1}^{M} y_m(x_i) - \prod_{m=1}^{M} y_m(x_j), 0 \right) \tag{14}$$

$$D(x_i) = \sum_{i \neq j}^{N} d_{ij} \tag{15}$$

$$\text{GGR}(x_i) = \frac{\text{GMR}(x_i)}{D(x_i)} \tag{16}$$

where x_i and x_j are two mutually different individuals in the space, M is the number of objectives, $D(x_i)$ is global density information of individual x_i, d_{ij} is the Euclidean distance between individual i and individual j, $\text{GMR}(x_i)$ is the global margin rank of individual x_i, and $\text{GGR}(x_i)$ is the global general rank of individual x_i. From the perspective of the Pareto dominant concept, a smaller $\text{GMR}(x_i)$ indicates that individual x_i dominates over other individuals. The degree of aggregation of individuals in the solution space is measured using Euclidean distances of an individual from remaining individuals in the population and the behavior of the individual to reduce effectively the impact of any extreme point or "outlier" on individual aggregation. Their combination results in a GGR, and a smaller GGR indicates that the individual is more dominant and that the individual density is small with a good distribution.

The framework of the proposed MOEA/D-AAU-GMR is given in Algorithm 1.

Simulation test and analysis

Solutions of MOEA/D-AAU-GMR

In this study, 14 features and 16 channels were selected as variables, 1950 training samples and 975 test samples were used, and the number of training cycles was 100. The lower

Algorithm 1. MOEA/D-AAU-GMR framework.

Input: N: population size, T: neighborhood size.
$B^i(T)$: index set of the neighbors of subproblem i.
d : a control parameter
G: angle control parameters
Begin
Initialization: P←{χ^i}// weight vectors Λ←{λ_i}
The ideal point Z^*←{ z_i^*}
Neighbor index set $B^i(T)$
Set $F^i=F(X^i)$, for i=1,2,…,N
while the termination condition is not met **do**
for each subproblem i =1,2,…,N **do**
E←determine the mating or updatepool(δ);
Randomly select indexes k,l from E to create new solution;
y←recombination operators(χ^k,χ^l);
P←population replacement (y);
End
Update external archive
end
return population P
end

Algorithm 2. MOEA/D-AAU-GMR population replacement.

Begin
for j←1 to N **do**
Compute the acute angle between α^j and ($F(y)$−Z^*)
i.e., $\theta(y)$=$\langle \alpha^j , F(y)-Z^* \rangle$
end
Select G minimum angle from N angle $\langle \alpha^j , F(y)-Z^* \rangle$
j=1,2,…,N and get
$\langle \alpha^{j1} , F(y)-Z^* \rangle \le \langle \alpha^{j2}, F(y)-Z^* \rangle \ldots \le \langle \alpha^{jG} , F(y)-Z^* \rangle$
for g←1to G **do**
if $F^{jg}(y) > F^{jg}(\chi_{jg})$ **then**
χ_{jg}←y
return
end
end

Algorithm 3. MOEA/D-AAU-GMR update external archive.

Begin
For each particle j in external archive **do**
Get the ranking values (Formula 14)
Get the density information (Formula 15)
Get the general ranking (Formula 16)
Sort by general ranking
Update external archive
Update Z^* by external archive
end

bound for the number of features was set to 4, and the lower bound for the number of channels was set to 6. Some solutions obtained to the Pareto front are shown in Figure 5.

Figure 5 was plotted based on four objective values of all Pareto front solutions: recognition accuracy, number of features, standard deviation of the action recognition rate, and number of channels from left to right, respectively. As can be seen in Figure 5, recognition accuracy varies much when the same number of channels and the same number of features are chosen. Because some solutions identical in number of channels and number of features do not use all the same features and channels, use of some features and channels might result in poor recognition of sEMG signals. Based on experimental results, for a majority of Pareto front solutions obtained, the mean recognition accuracy was >95%, and, for some solutions, the mean recognition accuracy of actions obtained reached 99.9%. In addition, for most Pareto front solutions, the standard deviations of action recognition accuracy were basically as low as 0.02 or so, implying that information in sEMG signals at selected features and channels can be effectively extracted to explore intrinsic regularity of each postural action, enabling each action to be recognized.

Not all the same features and channels are used by all Pareto front solutions, but some features or channels often play crucial roles and contain intrinsic regularity of actions. Consequently, most Pareto front solutions will recognize objectives by using sEMG signal information obtained from such types of features or channels. In the experiment, all obtained Pareto front solutions were analyzed; specifically, features and channels used by solutions were statistically analyzed to obtain usage rates of features and channels, as shown in Figures 6 and 7.

In Figures 6 and 7, each red rectangle indicates higher usage rate of a feature or channel. The usage rate of feature ZC (frequency of curves crossing zero, which mainly reflect changing characteristics of different frequency components of the sEMG signal) was 90.9%. This was much higher than that of any other features, which were 43.4%, 52.1%, and 43.3% for features root mean square (RMS), frequency ratio (FR), and integrated EMG (IEMG), respectively. The six highest ranked channels in usage rate were channels 1, 2, 8, 10, 12, and 16, respectively, with usage rates of 67.1%, 65.7%, 68.5%, 62.2%, 57.6%, and 80.4%, respectively.

Compared with other features, ZC represents the frequency of the sEMG signal magnitude crossing the zero magnitude level and reflects the degree of variation of the sEMG signal. An increase in ZC indicates more high-frequency components in the EMG signal while a decrease in ZC indicates more low-frequency components, so ZC is

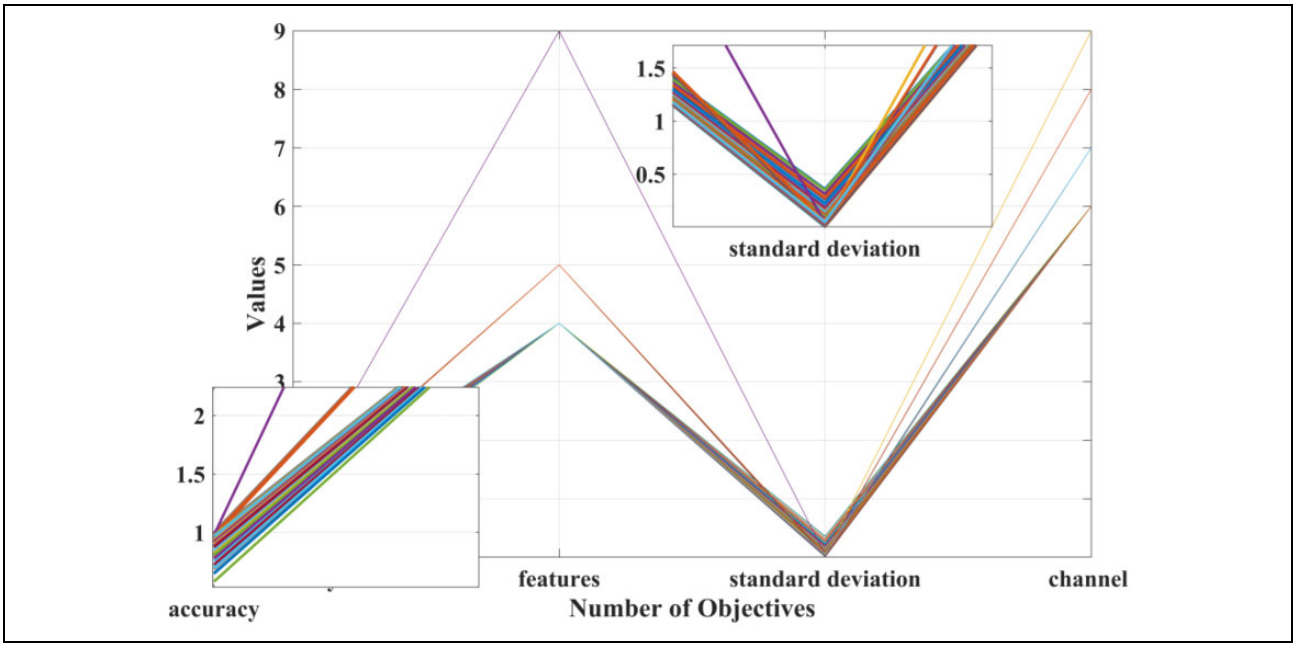

Figure 5. Results of objectives for MOEA/D-AAU-GMR.

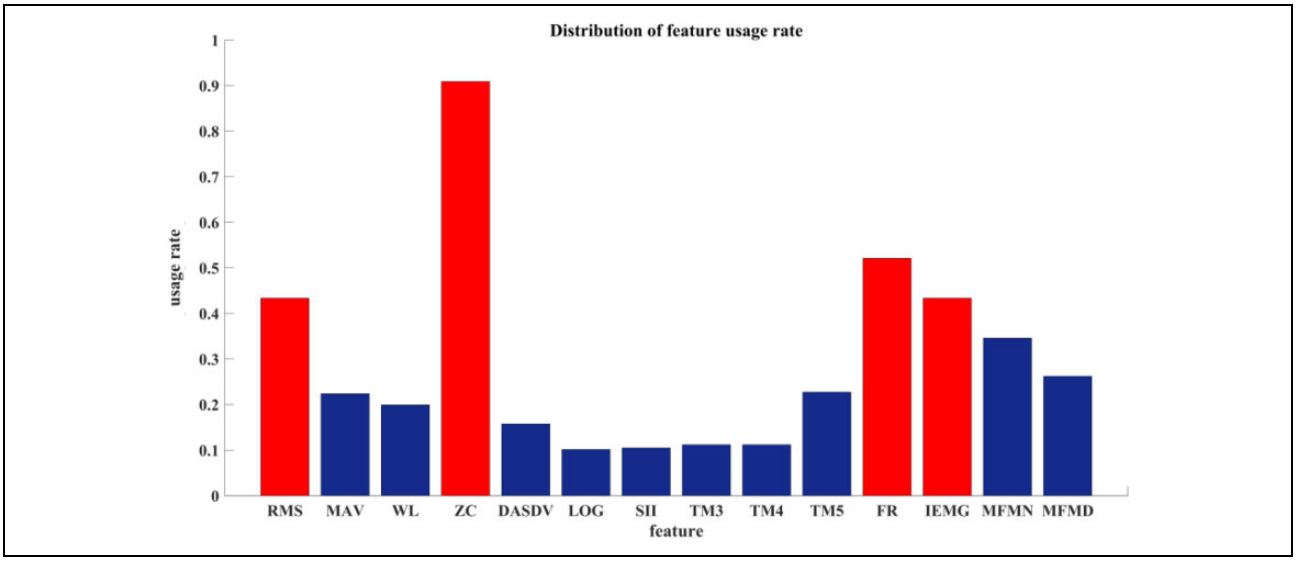

Figure 6. Distribution of feature usage rate.

mainly an indication of the changing features of each frequency component in the sEMG signal. The EMG signal per site varies constantly with time, and different actions need different myofiber sites. Consequently, differentiation in high-frequency or low-frequency components between channels becomes significant, and critical information can be better acquired with a classifier from frequency components of different channels of each action to discriminate actions, so the selection rate of the ZC feature will become very high. In addition, RMS, FR, and IEMG are able to reflect the amplitude of the sEMG signal, extent of muscle contraction and relaxation, and signal power, respectively. Compared with other features, such features are more capable of highlighting the essential regularity of the EMG signal, so Pareto front solutions have significantly higher selectivity of such features than that of other features. From the perspective of channel usage rate, human postures in daily living use different myofibers, and the six channels ranking highest in usage rate correspond to muscle sites capable of better reflecting the extent of contraction and relaxation of muscle masses used in different actions; hence, Pareto front solutions have higher selectivity of such channels. In general, even though highly discriminative features or channels reflecting

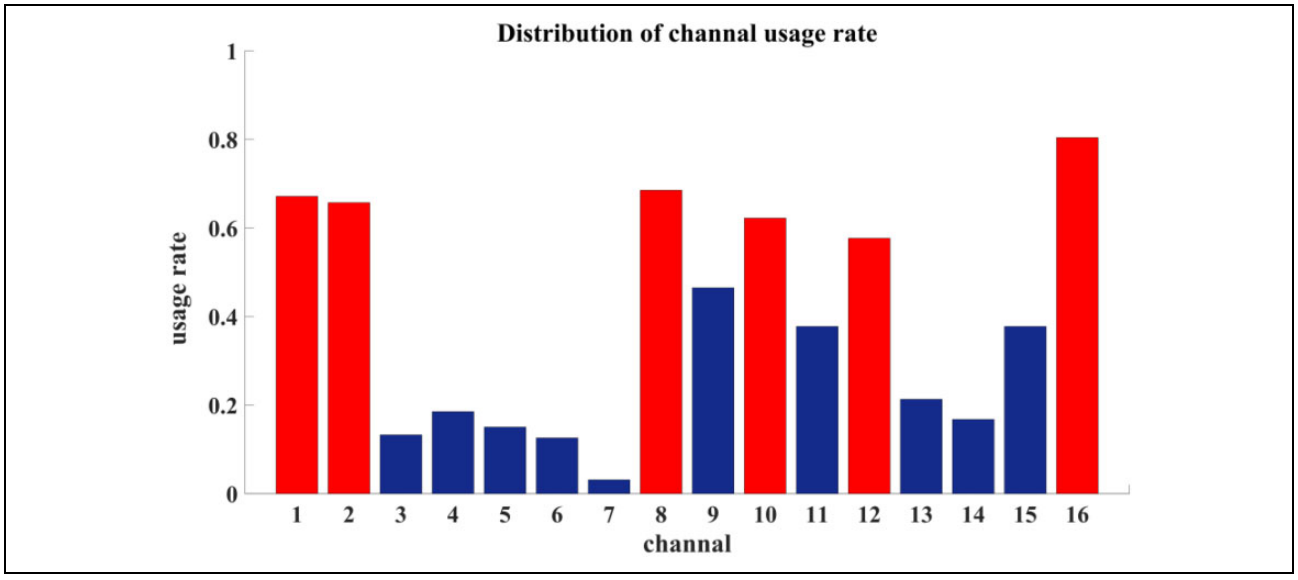

Figure 7. Distribution of channel usage rate.

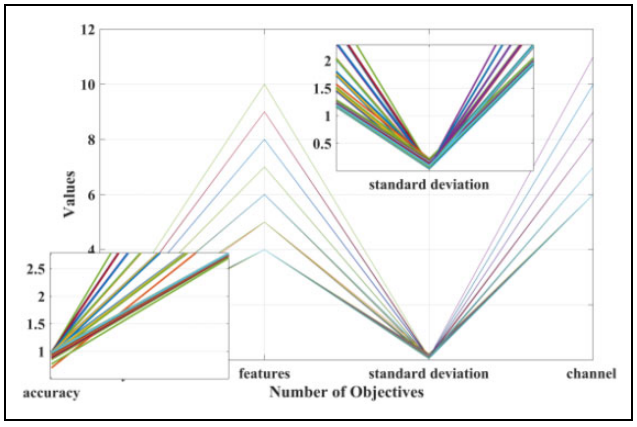

Figure 8. Results of objectives for MOEA/D. MOEA/D: decomposition-based multi-objective evolutionary algorithm.

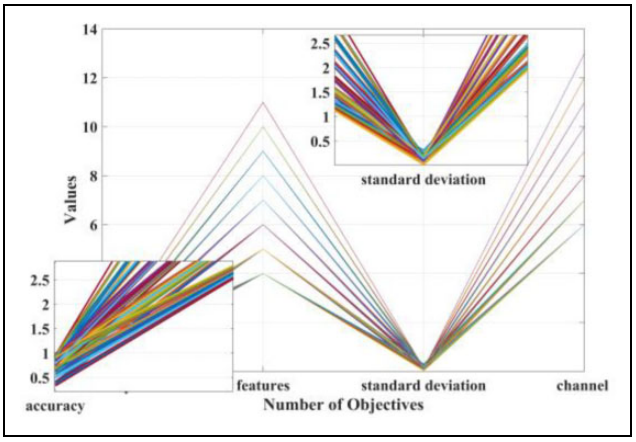

Figure 9. Results of objectives for MOEA/D-AU.

intense information of muscle mass contraction and relaxation are used, other features or channels can be used as a backup, in case abnormal EMG data are acquired in an experiment because of channel damage or recognition accuracy degradation owing to insufficient information contained in the features used.

Comparison between MOEA/D-AAU-GMR and other recognition methods

Under the same initial data and constraints, MOEA/D and MOEA/D-AU were used to solve the data set. The results are shown in Figures 8 and 9, respectively.

Figures 8 and 9 were plotted based on four objective values of all Pareto front solutions obtained by MOEA/D and MOEA/D-AU: recognition accuracy, number of features, standard deviation of the action recognition rate, and number of channels from left to right, respectively. Compared with the results from Figure 5, the solutions obtained by MOEA/D and MOEA/D-AU will still select greater numbers of features and channels, and recognition accuracy values derived from such solutions will remain low. Comparison of the three methods (MOEA/D, MOEA/D-AU, and MOEA/D-AAU-GMR) gives the diagrams of feature usage rate and channel usage rate shown in Figures 10 and 11, respectively.

Figures 10 and 11 show that the Pareto front solutions obtained by using the MOEA/D-AAU-GMR algorithm, compared with those obtained by using MOEA/D and MOEA/D-AU, have lower and more variable usage rates of features and channels, as detailed in Table 1. This implies that the whole front solutions obtained by using the MOEA/D-AAU-GMR algorithm focus on combinations of highly discriminative channels and features to improve recognition accuracy of such postural actions, thus somewhat decreasing usage rates.

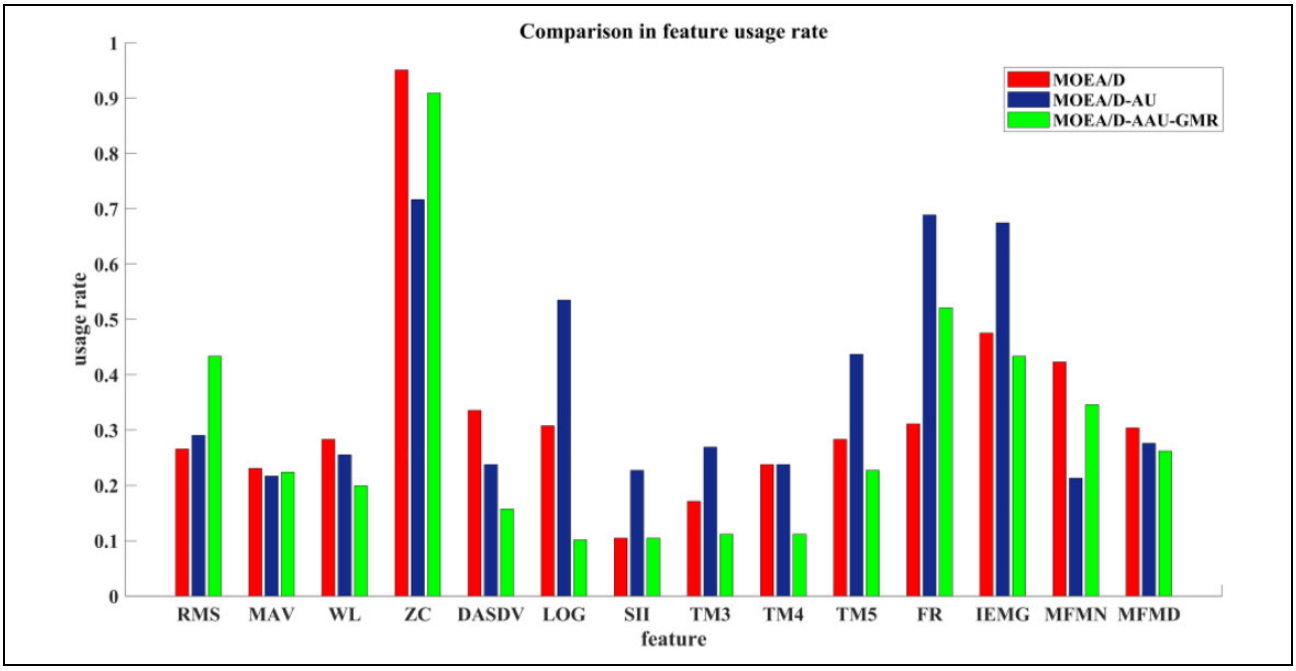

Figure 10. Comparison of feature usage rates.

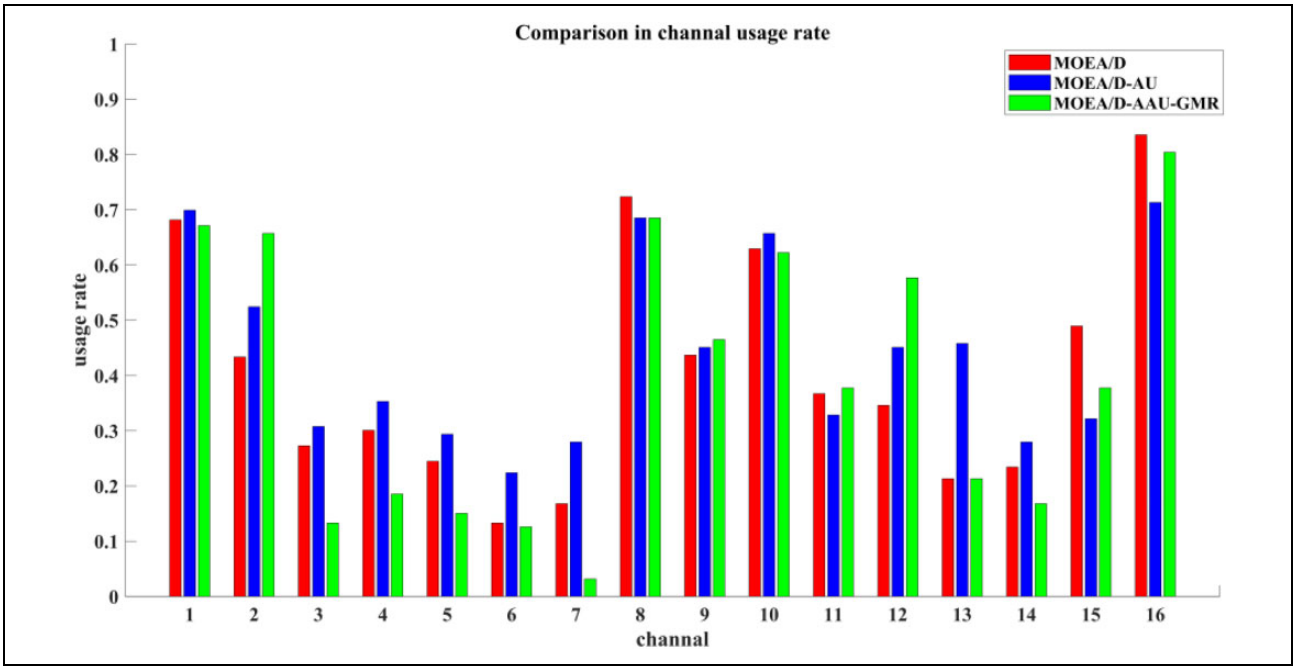

Figure 11. Comparison of channel usage rates.

As can be seen from Table 1, compared with MOEA/D and MOEA/D-AU, MOEA/D-AAU-GMR had a solution space with lower average feature usage rate and average channel usage rate but a greater variance. If a solution set obtained by an algorithm is closer to the Pareto front, then the objective values obtained by the solution set will be closer to a preset threshold value; hence, total numbers of features and channels used by the solution space will decrease constantly, and mean feature usage rate and mean channel usage rate will keep decreasing. This indicates that the Pareto front solutions selected by an algorithm are able to approximate consecutively the threshold value and are more capable of determining the importance of a feature or channel on postural actions in the sEMG signal. In summary, in terms of sEMG signal recognition, MOEA/D-AAU-GMR gives rise to Pareto front solutions

Table 1. Comparison among solutions derived from MOEA/D-AU, MOEA/D, and MOEA/D-AAU-GMR in feature and channel usage rates.

	Feature usage rate		Channel usage rate	
	Mean	Variance	Mean	Variance
MOEA/D	0.334	0.037	0.407	0.042
MOEA/D-AU	0.377	0.035	0.439	0.027
MOEA/D-AAU-GMR	0.296	0.046	0.390	0.059

MOEA/D: decomposition-based multi-objective evolutionary algorithm.

closer to the solution threshold so that the objective values can reach the threshold value.

A multi-objective algorithm can yield superior solutions at a lower cost and overcome the problem of a single-objective algorithm failing to cover all costs. In this study, with recognition accuracy as one objective, the ant colony algorithm was also employed to find the optimal solution to compare with the result of the multi-objective algorithm. Some of the optimal solutions are listed in Table 2, where the first three models are multi-objective algorithms while the last model is a single-objective algorithm. From the perspective of experimental results, solution sets obtained by using the multi-objective algorithms had superior performance in four objectives with minimal variations in action recognition. Although the ant colony algorithm ensured excellent recognition accuracy while the number of features and number of channels were small, the standard deviations of action recognition accuracy varied considerably, failing to ensure efficient recognition of each action, and an extreme case of high recognition accuracy of four actions but low recognition accuracy of one action may occur.

In summary, to optimize the EMG signal by single-objective programming, one neglects such factors as cost and action recognition heterogeneity, whereas modeling of an EMG signal by multi-objective programming can avoid such problems very well. By denoising the EMG signal data obtained from six channels at different positions and extracting four features from the denoised data, various gesture actions can be well recognized with minimal recognition errors. Moreover, using such features to recognize different actions resulted in minimal accuracy standard deviation, indicating that recognizing different actions leads to minimal difference without the extreme circumstance of four maxima and one minimum. Using fewer channels lowered hardware cost effectively and potentially reduced human discomfort. Using fewer features reduced the computational load, lowered cost, accelerated EMG signal recognition, and enabled real-time operation, laying a good foundation for future work on manipulating prosthetic limbs to accomplish preset actions.

Evaluation of multi-objective optimization algorithm

A coverage metric,[28] a spread metric,[29] and a spacing metric[30] were adopted to assess the multi-objective optimization algorithm and to evaluate the dominance ratio between the solution sets and the spread degree and uniformity of the solution's distribution.

A coverage metric was used to evaluate the ratio of the dominance of two solutions. For any two different Pareto fronts S_g and S_p, the coverage metric $C(S_g, S_p)$ is the proportion of elements in S_g that dominate the elements in S_p

$$\frac{C(S_g, S_p) = \left|\left\{y^p \in S_p \middle| \exists y^g \in S_g, y^g \prec y^p\right\}\right|}{\left|S_p\right|} \tag{17}$$

where $y^p = [y_1, y_2, \ldots, y_{na}]$ are the objectives that belong to Pareto front S_p, y^g are the objectives that belong to Pareto front S_g, and C lies between 0 and 1. Higher values of C indicate better dominance.

The spread metric D is used to evaluate the spread degree of the solution's distribution and is defined as

$$D = \sqrt{\sum_{k=1}^{n_o} \max\left(\left\|y_k^{\max} \bullet y_k^{\min}\right\|\right)} \tag{18}$$

where $y_k^{\max}$ is the maximum value of the kth target, $y_k^{\min}$ is the minimum value of the kth target, $\|\bullet\|$ is the Euclidean distance, and n_o is the number of objectives. When D is larger, the breadth of the algorithm is better.

The spacing metric SP is used to evaluate the uniformity of the solution's distribution and is defined as

$$\mathrm{SP} = \sqrt{\frac{1}{N-1}\sum_{l=1}^{N}\left(\bar{d} - d_l\right)^2} \tag{19}$$

where

$$\bar{d} = \frac{1}{N}\sum_{l=1}^{N} d_l \tag{20}$$

and

$$d_l = \min_j \left(\sqrt{\sum_{i=1}^{n_o}\left(y_i^l - y_i^j\right)^2}\right) l,\ j = 1, 2, ..., N \tag{21}$$

The smaller the value of SP, the better solution's distribution is. If $\mathrm{SP} = 0$, then the solved solution set is equidistantly distributed in the solution space.

We conducted experiments to obtain solutions using the three methods multiple times. The resulting coverage, spread, and spacing data are listed in Tables 3 and 4.

For the problem of sEMG signals, values of coverage between the solution set obtained by MOEA/D-AAU-GMR and those obtained by the two other algorithms were very close to 1, indicating that the solution set obtained by MOEA/D-AAU-GMR can dominate those obtained by MOEA/D and MOEA/D-AU well. Compared with solution

Table 2. Some optimal solutions to a problem.

Method	Features	Channels	Number of features	Number of channels	Recognition accuracy	Recognition standard deviation
MOEA/D	RMS, ZC, TM5, IEMG	2, 8, 9, 10, 12, 16	4	6	0.994	0.0396
	RMS, ZC, FR, MFMD	1, 2, 3, 8, 10, 16	4	6	0.988	0.0665
	ZC, DASDV, TM5, IEMG	1, 2, 8, 10, 12, 16	4	6	0.987	0.0572
	RMS, ZC, TM4, MFMN	2, 5, 9, 10, 15, 16	4	6	0.980	0.0705
MOEA/D-AU	ZC, TM5, FR, IEMG	1, 2, 8, 10, 13, 16	4	6	0.998	0.0004
	ZC, LOG, FR, IEMG	1, 8, 9, 10, 13, 16	4	6	0.997	0.0004
	ZC, TM5, FR, IEMG	1, 4, 5, 8, 10, 16	4	6	0.985	0.0554
	ZC, LOG, FR, IEMG	1, 8, 9, 10, 12, 16	4	6	0.988	0.0535
MOEA/D-AAU-GMR	ZC, FR, IEMG, MFMD	1, 2, 8, 10, 12, 16	4	6	0.998	0.0004
	ZC, FR, IEMG, MFMN	1, 2, 8, 10, 12, 16	4	6	0.998	0.0004
	RMS, ZC, FR, IEMG	2, 3, 9, 11, 12, 16	4	6	0.982	0.0334
	RMS, ZC, IEMG, MFMD	2, 8, 9, 10, 12, 16	4	6	0.990	0.0180
Ant colony algorithm	ZC, FR, IEMG, MFMN	1, 2, 7, 9, 12, 14	4	6	0.992	0.0550
	LOG, TM5, IEMG, MFMN	1, 2, 3, 8, 14, 16	4	6	0.972	0.0991
	ZC, TM5, FR, IEMG	2, 4, 6, 11, 13, 14	4	6	0.988	0.0755
	ZC, TM5, IEMG, MFMN	2, 5, 7, 10, 14, 15	4	6	0.982	0.0808

MOEA/D: decomposition-based multi-objective evolutionary algorithm; RMS: root mean square; ZC: zero crossing; MFN: modified frequency mean; DASDV: difference absolute standard deviation value; LOG: Log detector; TM3, TM4, TM5: absolute value of the 3rd, 4th, and 5th temporal moment.

Table 3. Comparison of the three methods in terms of coverage of the solution set.

	Coverage		
Method	MOEA/D	MOEA/D-AU	MOEA/D-AAU-GMR
MOEA/D	—	0.884 ± 0.135	0.901 ± 0.117
MOEA/D-AU	0.980 ± 0.032	—	0.902 ± 0.139
MOEA/D-AAU-GMR	0.988 ± 0.031	0.940 ± 0.106	—

MOEA/D: decomposition-based multi-objective evolutionary algorithm.

Table 4. Comparison of the three methods in terms of spread and spacing of solution sets.

Method	Spread	Spacing
MOEA/D	3.732 ± 0.165	0.159 ± 0.043
MOEA/D-AU	3.971 ± 0.081	0.283 ± 0.021
MOEA/D-AAU-GMR	2.570 ± 0.042	0.105 ± 0.071

MOEA/D: decomposition-based multi-objective evolutionary algorithm.

sets obtained by MOEA/D and MOEA/D-AU, the solution set obtained by MOEA/D-AAU-GMR was poorer in spread and much inferior to that obtained by MOEA/D-AU. However, in terms of spacing, the solution set obtained by MOEA/D-AAU-GMR converged at the Pareto front more uniformly with better effect. Numerical statistics on the spread and spacing metrics of the solution set were calculated in the experiment. Plots of the average, median, maximum, and minimum values are shown in Figures 12 and 13.

Based on Tables 3 and 4 and Figures 12 and 13, MOEA/D-AAU-GMR was superior to MOEA/D and MOEA/D-AU in coverage, spread, and spacing of the solution set. The solution set obtained by MOEA/D-AAU-GMR dominated those obtained by MOEA/D and MOEA/D-AU well, being closer to the Pareto fronts with a more uniform distribution, though its spread was slightly insufficient. In summary, the use of MOEA/D-AAU-GMR was effective.

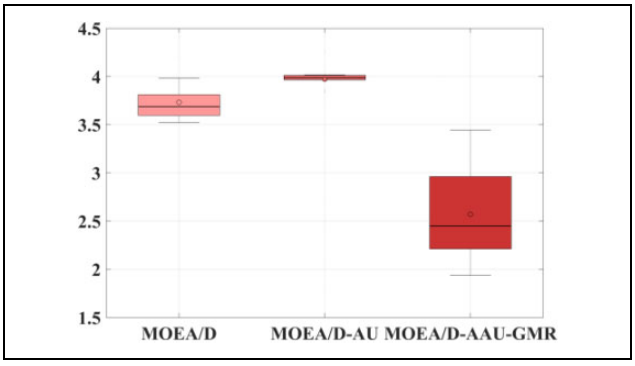

Figure 12. Spread metric statistics of solutions.

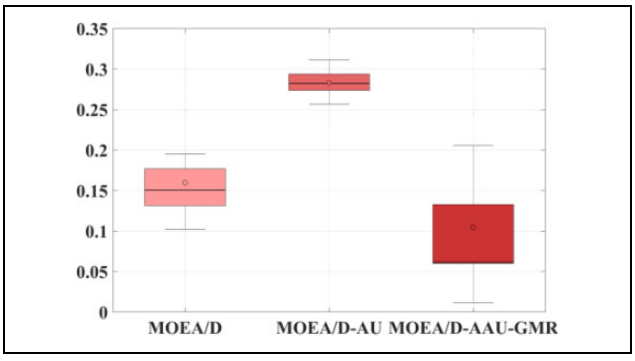

Figure 13. Spacing metric statistics of solutions.

Table 5. Channels for most Pareto solutions versus channels for a single optimal solution.

	Accuracy	
Channels	Electrode shift	Interpersonal
1, 2, 8, 10, 12, 16	70.7%	60.9%
2, 3, 9, 11, 12, 16	71.1%	59.5%

Validity check

To verify that the channels for most of the Pareto solutions obtained above are valid, we compared the top six channels (1, 2, 8, 10, 12, and 16) ranked in usage rate against channels for the first solutions in Table 3. The validity of the channels was checked from two aspects, namely, electrode shift-induced recognition accuracy and interpersonal recognition accuracy. Because a test unit was worn at positions varying with time, a muscle site under test remaining completely unchanged could not be assured. In addition, EMG signals differ from person to person, so it is imperative to ensure that such channels have good recognition accuracy in recognizing actions of different persons. The following protocols were used:

(1) EMG data of one person measured in the morning and in the afternoon were used to detect the effects of electrode shift on recognition accuracy. The EMG data acquired in the morning served as the training set while the EMG data acquired in the afternoon served as the test set.
(2) EMG data of different actions from multiple persons were used to recognize interpersonal action accuracy.

Introducing these data into a neural network for training recognition gives the results listed in Table 5.

The test results for both aspects are very similar, with channels for most Pareto solutions being slightly lower than those for a single optimal solution but channels selected by optimal solutions varying with objective weight. Using channels for most Pareto solutions eliminates the need of recalculating the optimal channel and is thus applicable to objectives at most weights, which greatly reduces computational cost of recalculating the optimal channel because of the weight change. The development of prosthetic limbs in the future has to focus on different aspects, and it will be unnecessary to recalculate channels resulting from frequent changes of foci, indicating that channels for most Pareto solutions obtained in a multi-objective model are valid.

Conclusions

EMG signals have been modeled by multi-objective programming. Problems such as cost and action recognition heterogeneity have been considered, and maximized average recognition accuracy of different actions and minimized difference in recognition of different actions were ensured while numbers of features and channels were minimized. After lower bounds on the numbers of features and channels were set, a multi-objective optimization algorithm based on decomposition was used to solve for the optimal Pareto front.

For all Pareto front solutions, usage rates of features ZC, RMS, FR, and IEMG were high, with channels 1, 2, 8, 10, 12, and 16 being highest ranked in usage rate, respectively, and most solutions gave a recognition accuracy of >95%. In EMG signal optimization by single-objective programming, it is easy to neglect factors such as cost and action recognition heterogeneity, whereas EMG signal modeling by multi-objective programming can avoid these problems very well. Compared with other features, ZC mainly reflects the changing features of different frequency components of the sEMG signal. Different actions need different myofiber sites, so differentiation between high-frequency and low-frequency components would be significant for EMG signals acquired at different channels, and a classifier is more capable of obtaining critical information to discriminate actions.

To improve the distribution of solutions, MOEA/D-AAU-GMR was employed in solution finding. Its solution had a wider coverage and was closer to critical values of solutions at different objective weight vectors. The validity of channels for most Pareto solutions was checked from two aspects, namely, electrode shift-induced recognition accuracy and interpersonal recognition accuracy. Their accuracy values of 70.7% and 60.9%, respectively, are very similar to the results of an optimal solution, though the cost of recalculating the optimal channel when the objective weight changes was reduced.

Declaration of conflicting interests

The author(s) declared no potential conflicts of interest with respect to the research, authorship, and/or publication of this article.

Funding

The author(s) disclosed receipt of the following financial support for the research, authorship, and/or publication of this article: This work was partly supported by the National Natural Science Foundation of China (Nos 61873240 and 51875524) and the Open Fund of the Key Laboratory for Metallurgical Equipment and Control of the Ministry of Education at the Wuhan University of Science and Technology (No. 2017B04).

ORCID iD

Guoqi Chen https://orcid.org/0000-0003-3179-9735

References

1. He B, Wang S, and Liu YJ. Underactuated robotics: a review. *Int J Adv Rob Syst* 2019; 16(4): 1–29.

2. He B, Shao Y, Wang S, et al. Product environmental footprints assessment for product life cycle. *J Clean Prod* 2019; 233: 446–460.
3. Kang HS, Lee JY, Choi S, et al. Smart manufacturing: past research, present findings, and future directions. *Int J Precis Eng Manuf-Green Technol* 2016; 3: 111–128.
4. Shah R and Ward PT. Lean manufacturing: context, practice bundles, and performance. *J Oper Manage* 2003; 21: 129–149.
5. Zhang L, Luo Y, Tao F, et al. Cloud manufacturing: a new manufacturing paradigm. *Enterp Inf Syst* 2014; 8(2): 167–187.
6. Tao F, Cheng Y, Zhang L, et al. Advanced manufacturing systems: socialization characteristics and trends. *J Intell Manuf* 2017; 28(5): 1079–1094.
7. Cai J, Hu Y, and Zhang Y. An improved random retreat DBN recognition method for EEG signals. *J Harbin Inst Technol* 2018; 50: 186–190 (in Chinese).
8. Tian X, Sun Z, Xu B, et al. Recognition of body sEMG signal gesture based on LabVIEW. *Lab Sci* 2018; 21: 71–74 (in Chinese).
9. Lu L and Liu S. Application of non-linear SVM and LDA in sEMG gesture recognition. *Laser J* 2014; 35: 26–29 (in Chinese).
10. Cai L, Wang Z, and Liu Y. Modeling and classification of two channel electromyography signals based on blind channel identification theory. *J Shanghai Jiaotong Univ* 2000; 34: 1471–1474 (in Chinese).
11. Cai L, Wang Z, and Zhang H. Surface EMG signal classification using wavelet transform. *J Biomed Eng* 2000; 17: 281–284 (in Chinese).
12. Nazarpour K. *Brain signal analysis in space-time-frequency domain: an application to brain computer interfacing*. Cardiff University, UK, 2008.
13. Zhang Q, Li H, Maringer D, et al. MOEA/D with NBI-style Tchebycheff approach for portfolio management. In: *Proceedings of the 2010 6th IEEE World Congress on Computational Intelligence, WCCI 2010 - 2010 IEEE Congress on Evolutionary Computation(CEC)*, Barcelona, Spain, 18–23 July 2010, pp. 1–8. IEEE.
14. Trivedi A, Srinivasan D, Pal K, et al. A MOEA/D with non-uniform weight vector distribution strategy for solving the unit commitment problem in uncertain environment. In: *Australasian conference on artificial life and computational intelligence*, Geelong, Australia, 31 January–2 February 2017, pp. 378–390, Cham, Switzerland: Springer.
15. Suciu M, Pallez D, Cremene M, et al. Adaptive MOEA/D for QoS-based web service composition. In: *European conference on evolutionary computation in combinatorial optimization*, Vienna, Austria, 3–5 April 2013, pp. 73–84. Berlin, Heidelberg: Springer.
16. Zapotecas-Martínez S, Derbel B, Liefooghe A, et al. Injecting CMA-ES into MOEA/D. In: *Proceedings of the 2015 annual conference on genetic and evolutionary computation (ed S Silva)*, Madrid, Spain, July 2015, pp. 783–790. New York: ACM.
17. Zhao SZ, Suganthan PN, and Zhang Q. Decomposition-based multiobjective evolutionary algorithm with an ensemble of neighborhood sizes. *IEEE Trans Evol Comput* 2012; 16(3): 442–446.
18. Qi Y, Ma X, Liu F, et al. MOEA/D with adaptive weight adjustment. *Evol Comput* 2014; 22(2): 231–264.
19. Jiang S and Yang S. An improved multiobjective optimization evolutionary algorithm based on decomposition for complex Pareto fronts. *IEEE Trans Cybern* 2015; 46(2): 421–437.
20. Yin PY, Wu TH, and Hsu PY. Simulation based risk management for multi-objective optimal wind turbine placement using MOEA/D. *Energy* 2017; 141: 579–597.
21. Li H and Zhang Q.Multiobjective optimization problems with complicated Pareto sets, MOEA/D and NSGA-II. *IEEE Trans Evol Comput* 2009; 13: 284–302.
22. Zhang Q and Hui L. MOEA/D: a multiobjective evolutionary algorithm based on decomposition. *IEEE Trans Evol Comput* 2008; 11: 712–731.
23. Žalik KR and Žalik B. Multi-objective evolutionary algorithm using problem-specific genetic operators for community detection in networks. *Neural Comput Appl* 2017; 30: 2907–2920.
24. Wang L and Zhang Q. Constrained subproblems in a decomposition-based multiobjective evolutionary algorithm. *IEEE Trans Evol Comput* 2016; 20: 475–480.
25. Liu J, Li X, Li G, et al. EMG feature assessment for myoelectric pattern recognition and channel selection: a study with incomplete spinal cord injury. *Med Eng Phys* 2014; 36: 975–980.
26. Ying S, Li L, Wang Z, et al. An improved decomposition-based multiobjective evolutionary algorithm with a better balance of convergence and diversity. *Appl Soft Comput* 2017; 57: 627–641.
27. Li L, Wang W, and Xu X. Multi-objective particle swarm optimization based on global margin ranking. *Inform Sci* 2017; 375: 30–47.
28. Zitzler E and Thiele L. Multiobjective evolutionary algorithms: a comparative case study and the strength Pareto approach. *IEEE Trans Evol Comput* 1999; 3: 257–271.
29. Zitzler E, Deb K, and Thiele L. Comparison of multiobjective evolutionary algorithms: empirical results. *Evol Comput* 2000; 8: 173–195.
30. Schott JR. *Fault tolerant design using single and multicriteria genetic algorithm optimization*. Air Force Inst of Tech Wright-Patterson AFB, 1995.